

# Observation of shear band formation in nanocrystalline Pd–Au alloy during in situ SEM compression testing

Yulia Ivanisenko · Thomas Werz · Alexander Minkow ·  
Jochen Lohmiller · Patric A. Gruber · Aaron Kobler ·  
Lilia Kurmanaeva · Hans-Jörg Fecht

Received: 8 March 2013 / Accepted: 30 May 2013 / Published online: 15 June 2013  
© Springer Science+Business Media New York 2013

**Abstract** Understanding the deformation behavior of nanocrystalline (nc) materials is important because of their possible application as structural materials. The investigation of macroscopic nc samples during in situ mechanical tests can shed light on operating deformation mechanisms. For example, observations during a compression test in a scanning electron microscope (SEM) or results obtained by more localized methods like transmission electron microscopy can extend our knowledge on this subject. In this study, we present the results of in situ SEM compression tests on nc Pd–10 at.% Au alloy with a mean grain size of 23 nm produced using the combination of inert gas condensation with subsequent high-pressure torsion. We show that plastic flow in this material is very inhomogeneous on both the macro and the mesoscale as it is localized in one area of the compression sample and within

shear bands. The formation of shear bands is accompanied by strain softening. We propose that such behavior can be explained by the activation of grain boundary mediated deformation mechanisms instead of dislocation-based plasticity. This conclusion was supported by in situ synchrotron XRD measurements which revealed that no preferential grain orientation is forming during the compression of identically prepared samples of the same material.

## Introduction

Understanding of the deformation behavior of nanocrystalline (nc) materials is important in view of their possible application as structural materials. In the last three decades, numerous experiments have been performed, and evidence has been obtained that confirms the operation of various deformation mechanisms in such materials like grain boundary sliding [1–3], grain rotation [4–6], diffusional creep [7], twinning [8–10], partial dislocation nucleation from grain boundaries (GBs), and related stacking fault formation [11, 12]. Due to a low-strain hardening capacity, nanostructured materials are prone to strain localization in shear bands [13–16]. Deformation behavior of nanocrystalline materials has been summarized in several review articles, see for example Refs. [12, 17–20]. Despite extensive research, there is still a lack of understanding in regard to the deformation mechanisms operating in such materials. For example, various deformation mechanisms were recognized using in situ TEM straining of thin nc metal foils. To mention some, Hugo et al. [21] reported the emission of dislocation segments from the grain boundaries, Shan et al. [5] and Kobler et al. [22] reported grain rotation accompanied by twinning and detwinning. On the

---

Y. Ivanisenko (✉) · A. Kobler  
Institute for Nanotechnology, Karlsruhe Institute for Technology  
(KIT), 76021 Karlsruhe, Germany  
e-mail: julia.ivanisenko@kit.edu

T. Werz · A. Minkow · H.-J. Fecht  
Institute of Micro and Nanomaterials, Ulm University,  
89081 Ulm, Germany

J. Lohmiller · P. A. Gruber  
Institute for Applied Materials, Karlsruhe Institute for  
Technology (KIT), 76021 Karlsruhe, Germany

A. Kobler  
Joint Research Laboratory Nanomaterials (KIT and TUD)  
at Technische Universität Darmstadt (TUD), Petersenstr. 32,  
64287 Darmstadt, Germany

L. Kurmanaeva  
Department of Chemical Engineering & Materials Science,  
University of California Davis, Davis, CA 95616, USA

other hand, Rösner et al. [23] observed the fracture along grain boundaries without any apparent plastic deformation. Despite the advantage of observing the ongoing processes in the material in situ, TEM provides only local information about the mechanism that controls the plastic flow. Further, the investigation may suffer from artifacts due to the high-surface-to-volume ratio of the TEM sample. In situ XRD synchrotron measurements, on the other hand, have the advantage to probe the volume averaged material behavior and, therefore, provide better statistics than TEM. In many cases, the analysis of peak broadening during straining of nc samples indicated dislocation activity [24]. On the other hand, texture measurements of nanocrystalline samples after significant strain revealed weak or no texture formation. This is an indication that dislocations contribute only moderately to plastic flow [25, 26]. There is, therefore, a need for further experiments with the other methods. In the past, the deformation mechanisms in metals and alloys were frequently investigated by observing the deformation relief development. Due to the limited sample dimensions (usually nc materials are obtained in the form of thin films), such investigations are often difficult in nc materials. Nanocrystalline samples produced by inert gas condensation (igc) [27] have a very uniform microstructure and a grain size as small as 10–15 nm. Their dimensions are large enough to perform conventional tensile and compression tests. There is some porosity (up to 7 %) in as igc samples, however, subsequent processing by high-pressure torsion (hpt) allows the increase of relative density up to 98 % [28]. In this study, we present our results on two in situ compression tests of hpt-processed igc Pd–10 at.% Au alloys: an in situ SEM observation of surface relief development, and an in situ synchrotron diffraction experiment with subsequent peak profile analysis. We show that the development of shear bands is the dominating mechanism of plastic deformation in this material.

## Experimental

Nanocrystalline Pd–10 at.% Au samples (later called: Pd10Au) with a mean grain size of 13 nm [29] with a diameter of  $d = 8$  mm and a thickness of  $t = 1$  mm were produced by inert gas condensation using the parameters and procedures as described in Refs. [27, 29]. As-igc samples were further processed by hpt for one full rotation ( $2\pi$ ) at a constant rotation speed of  $2\pi$  per minute and a pressure of 6 GPa using a custom built computer controlled hpt device (W. Klement GmbH, Lang, Austria). The shear strain at the sample radius of  $R = 2.5$  mm calculated as  $\gamma = 2\pi R/t$  was 15.7. The microstructure of comparable samples was previously studied in Ref. [25]. A typical dark

field image of the microstructure is shown in Fig. 1a, and the grain size distribution is shown in Fig. 1b. One can see that the mean grain size increased after hpt to  $23 \pm 2$  nm.

For the miniature compression tests, samples of a cuboid geometry with dimensions of  $0.8 \times 0.8 \times 1.5$  mm<sup>3</sup> (compression along the long axis) were cut out from the hpt disc at a distance from its center of 2.5 mm. Successive mechanical polishing steps with colloidal silica of decreasing particle sizes have ensured sufficient smoothness of the sample surface. In situ compression tests were conducted using a constant strain rate of  $5 \times 10^{-4}$  s<sup>-1</sup> with a testing apparatus MicroDAC (Kammrath and Weiss GmbH, Dortmund, Germany), which was installed in a high-resolution field-emission scanning electron microscope (FE-SEM) LEO 1550. The load–elongation curves and a sequence of images were recorded during the deformation process. In order to reveal the macroscopic features of the surface relief, the polished sample surface was covered with a thin carbon film that enhances the imaging contrast of the SEM. For comparison, a Cu sample with a mean grain size of 64  $\mu$ m was polished and coated in the same way as the nanocrystalline Pd10Au sample. Subsequently, both the samples were compressed in the SEM up to 20 % compressive strain.

Microstructural investigations were performed after in situ compression test using FEI Tecnai F20 operated at 200 kV. TEM samples were FIB-cut parallel to the compression axis. The mean grain size was estimated by measuring two perpendicular diameters of individual grains in at least five arbitrarily selected typical dark field TEM images. Each image contained at least 60 grains in Bragg condition.

In addition to the in situ SEM experiments, an in situ XRD compression test was conducted on an identically prepared sample of the same material using a synchrotron-based mechanical testing setup [30]. The experiment was carried out at the high-energy micro diffraction endstation of beamline ID15A at the ESRF. The setup comprises a mechanical testing device (Kammrath and Weiss, Dortmund, Germany) mounted in transmission geometry and a large area detector (MarCCD 165, Marresearch Inc., Evanston, IL, USA). Due to the high-X-ray energy of 69.7 keV, the X-rays can penetrate through several hundred microns thick sample yielding excellent statistics and a sufficient signal-to-noise-ratio. In order to obtain the distribution of crystallographic orientations within the plane perpendicular to the X-ray beam, the integral peak intensity along several Debye–Scherrer rings was analyzed by radial scans along the diffraction angle  $2\theta$  in individual azimuthal directions  $\Phi$  with an azimuthal increment of  $\Delta\Phi = 2^\circ$ .

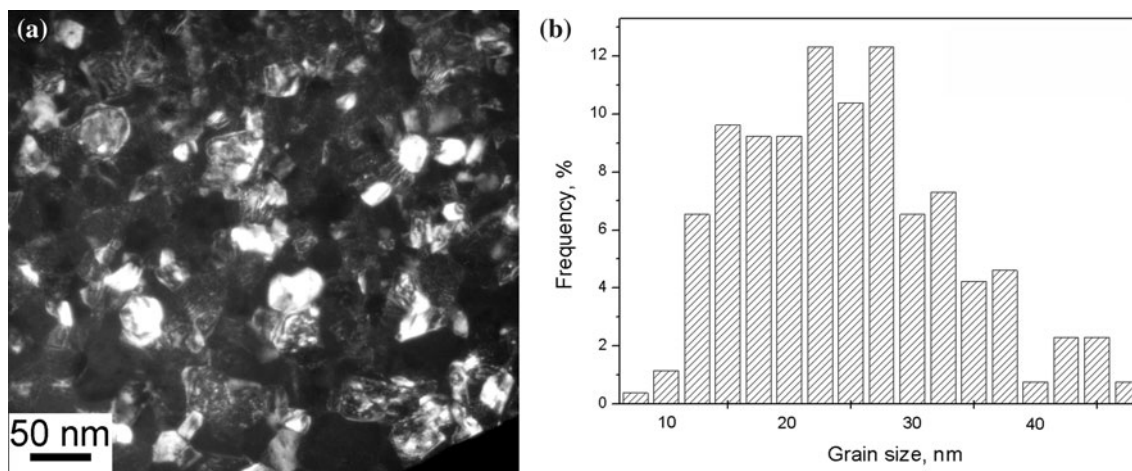


**Fig. 1** **a** Typical dark field TEM image of the microstructure of nc Pd10Au alloy after igt and subsequent hpt straining at  $\gamma = 15$  (image plane = hpt disk plane). **b** Corresponding grain size distribution histogram. Reprinted from [15] with permission of Springer

## Results and discussion

A typical compression, true stress–strain compression curve of an igt + hpt processed Pd10Au sample is shown in Fig. 2. The initial portion of the curve within the first 4 % of plastic strain has a parabolic shape with a very smooth transition between linear elastic and plastic behavior. Remarkably, despite the large amount of strain imposed to the sample during the previous hpt processing, the sample still demonstrated notable strain hardening with a yield ratio of  $\sigma_p/\sigma_m = 0.43$ , where  $\sigma_p$  is the proportionality limit, and  $\sigma_m$  is the maximal applied stress. An extended parabolic hardening regime was also observed in shear compression tests [31], and in tensile tests of free standing nanocrystalline films of the same material [32, 33] as well as tensile tests of electrodeposited Ni [34]. The in situ synchrotron XRD analysis [32–34] together with the analysis of deformation curves [31–33] show that this stage corresponds to the transition from elastic to fully plastic behavior, i.e., this corresponds to the microplastic stage. After achieving  $\sigma_m = 1630$  MPa, the applied stress starts to decrease indicating strain softening. Such behavior with low or negative strain hardening is typical for many nanostructured and ultrafine grained bcc and fcc materials as for example Fe [14], Cu [15], and Ni [35]. Finally, the sample fractured after plastic strain of 9 %.

The development of the deformation relief on the sample surface during the compression test was observed using several identically processed samples. They all showed essentially similar behavior. In these tests, several pauses had been made during the compression to take the SEM images. During these pauses, notable stress relaxation occurred. However, the envelope of the corresponding compression curve (not shown here) was very similar to that recorded in the continuous test (Fig. 2). Figure 3a–c

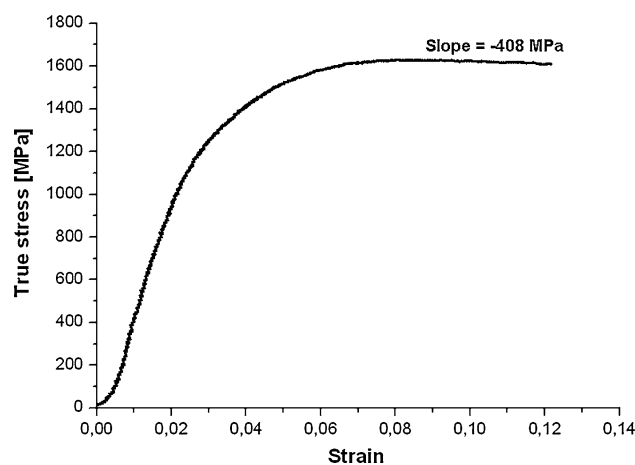


**Fig. 2** True stress/strain compression curve of nanocrystalline igt + hpt Pd10Au sample

shows the compression specimen at 0, 6, and after fracture at about 10 % strain. One can see that the deformation of the sample proceeded very inhomogeneously: Starting from 6 % strain, a bulge started to grow at the left-hand upper side of the sample (see arrow in Fig. 3b) and, after 8 % strain, deformation in the right side stagnated completely (thickness was not increasing any more until fracture). Careful inspection of the sample did not reveal any traces of plastic deformation on its surface during the microplastic stage: The surface remained smooth and the carbon film was not damaged (Fig. 4a). First surface defects were visible in the form of short cracks in the carbon film (Fig. 4b), and occurred only for plastic strains of more than 6.5 %. With further increase of strain, shear bands (SBs), inclined at  $45^\circ$  to the compression axis, started to propagate gradually (Fig. 4c, d). Finally, shear bands covered the sample surface along a wide diagonal stripe spreading from the lower left- to upper right-hand

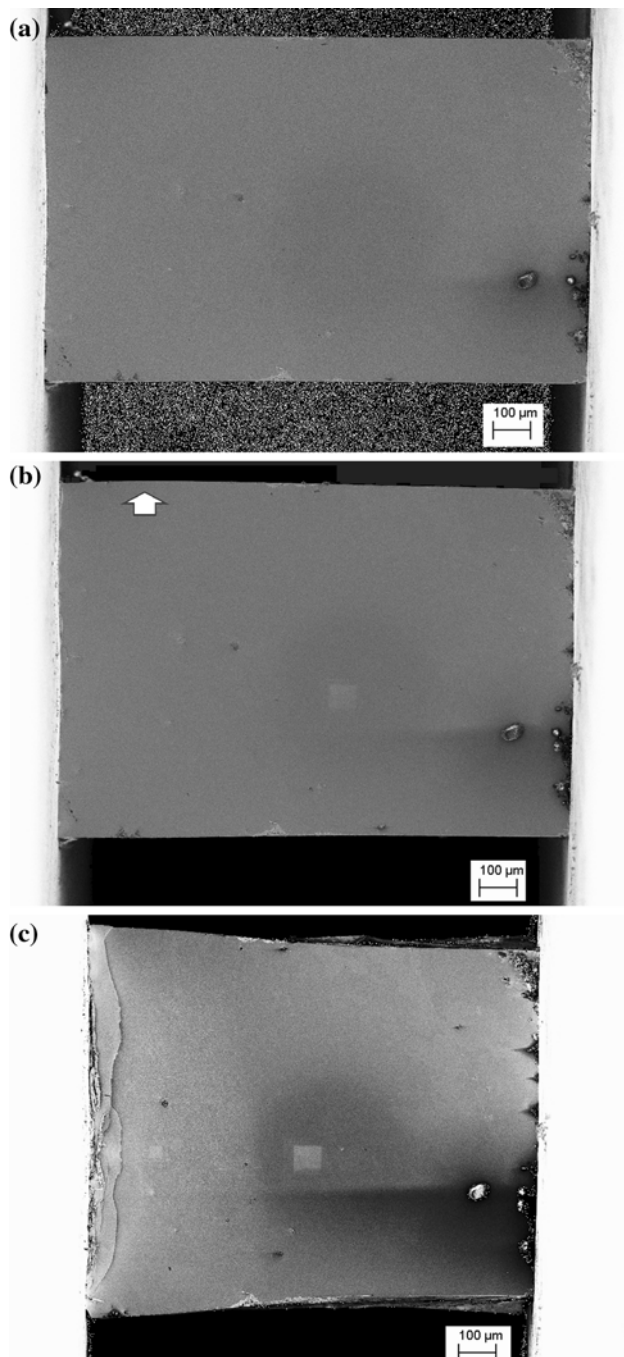


**Fig. 3** SEM images taken during in situ compression test: view of the specimen at **a** 0 % strain, **b** 6.5 % strain, and **c** after fracture (10 % strain). Compression direction is horizontal

corner of the sample. Fracture took place at a compressive strain of about 10 % (Fig. 4e). Multiple cracks were formed in areas of localized plastic flow within SBs (Fig. 4f). At higher magnifications (Fig. 4g), it was observed that shear bands were visualized as up to 1- $\mu\text{m}$  thick bundles of fine cracks within the carbon film. These fine cracks spread for tens and hundreds of microns. The

distance between individual SBs varied from 3 to 10  $\mu\text{m}$ . Observation of kinks at the polishing scratch lines in areas where they were intersected by shear bands (Fig. 4g) revealed that related displacements can be up to 1  $\mu\text{m}$  large. Due to insufficient statistics, we were not able to estimate the strain which was carried by shear bands.

In contrast to the deformation relief appearance in the Pd10Au sample (Fig. 4), the surface of the similarly compressed coarse-grained Cu sample was fully covered with slip lines. According to the operating crystallographic slip system, slip lines were individually oriented in each grain nicely documenting the development of dislocation slip (Fig. 5).

Remarkably, TEM microstructure investigations had not revealed any notable changes in the grain shape and grain size distribution after compression test of igc + hpt sample and only slight increase of the mean grain size from  $23 \pm 2$  to  $27 \pm 2$  nm due to stress induced grain growth [22, 28, 36] (compare Figs. 1a, b, 6a–c), despite the FIB lamella was taken in the area with maximal density of shear bands. Note that our previous report on the microstructure investigation of pure nc Pd and Pd10Au alloy also did not reveal any changes of the grain shape after high-pressure torsion [25, 28]. Conversely, planes of cooperative grain boundary sliding were observed in both cases.

Finally, we analyzed the deformation behavior of the igc + hpt Pd10Au sample using synchrotron-based compression testing. The sample was taken from the same production batch as the samples for the in situ SEM tests. The polar plot in Fig. 7 shows the modulation of the (111) integral peak intensity along the Debye–Scherrer ring. After more than 10 % strain, only a slight sixfold symmetry evolved. This is distinctively less pronounced as compared to similar experiments on nc Nickel with 30-nm grain size [30]. An emerging sixfold symmetry of the (111) integral intensity indicates the formation of a specific in plane texture. It is typically found for ductile coarse-grained fcc materials during compression. Therefore, it is argued that the igc + hpt Pd10Au sample has a weak contribution of dislocation glide to the overall deformation.

The in situ observation on the sample surfaces during compression tests have shown that soon after the onset of fully plastic deformation, the deformation becomes very inhomogeneous on both, the macro and the mesoscale. The deformation is localized in only one part of the compression sample and within the shear bands. This may explain the strain softening seen in the deformation curve. Please note that this occurs simultaneously with the detection of first shear bands. The propagation of shear bands often leads to strain softening as e.g., in coarse-grained materials [37]. However, strain softening takes place at high strains and/or high-strain rates. Under these conditions, intragranular dislocation slip leads to grain rotation toward



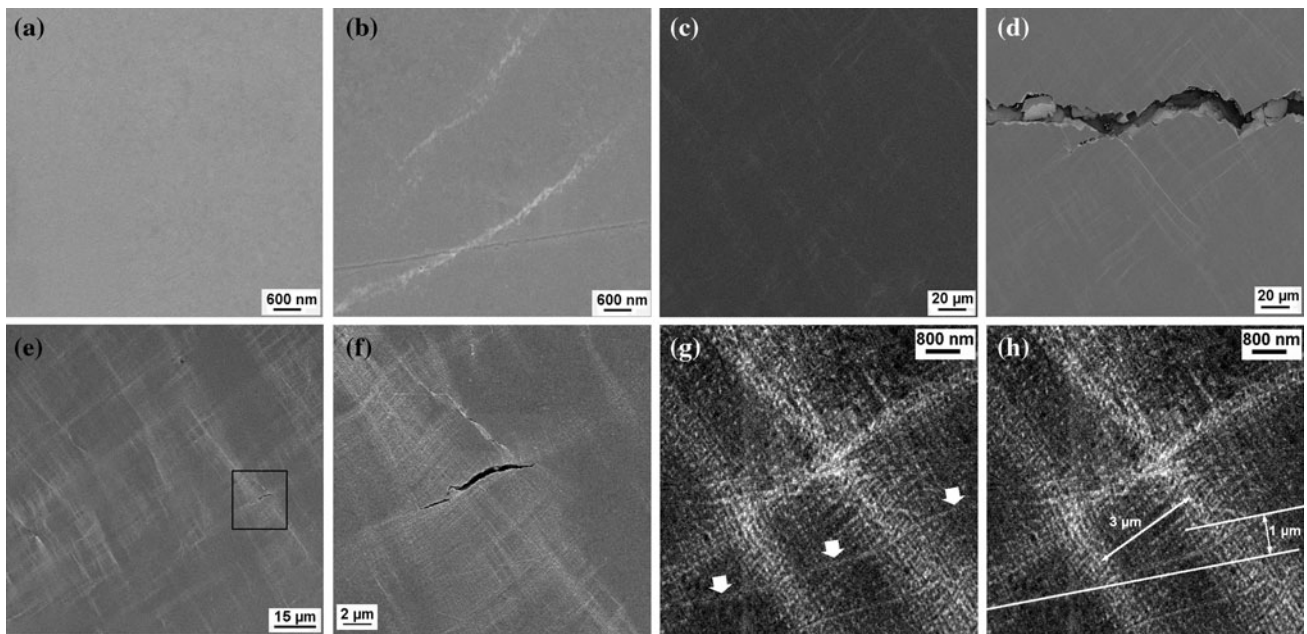


**Fig. 4** The development of the surface relief at **a** 4 % strain, **b** 6.5 % strain, first cracks in the carbon film are visible, **c** 7.5 % strain, first shear bands inclined at 45° to compression axis become visible, **d** 8.5 % strain, appearance of first surface macrocracks and further SB formation, **e** 10 % strain, fracture; **f** enlarged image of the rectangular area in **e** showing formation of a big crack and several small ones in

areas with high density of SB, **g** 10 % strain, enlarged image of shear bands, arrows highlight a polishing scratch kinked at its cross section with two shear bands, **h** the same image as in **g** showing that displacement related with shear bands can achieve 1 μm at a distance of 3 μm. Compression direction is horizontal in all images

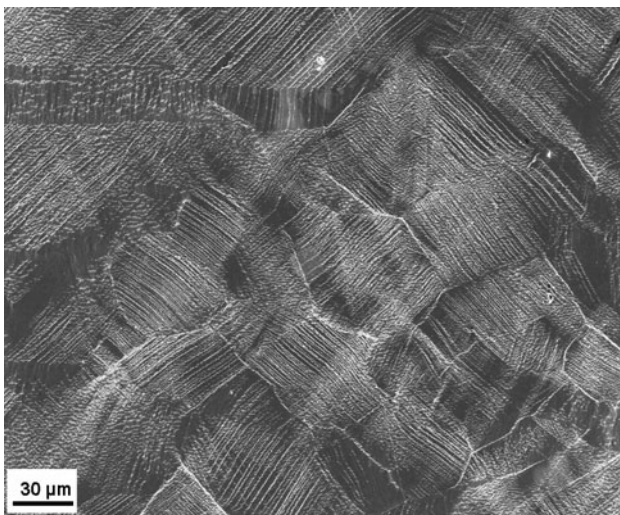


**Fig. 5** Deformation relief in Cu sample with a mean grain size of 64 μm after compression for 20 %

stable texture orientations. Hence, the grains become more or less aligned with each other. The evolving crystallographic texture helps to promote the localization process, as the lattice misorientations along the grain boundaries are reduced and cooperative slip of neighboring grains is facilitated [38]. Formation of shear bands has been reported in many nanocrystalline materials, however, these materials have larger grain size [14–16]. In particular, the

inspection of microstructure within shear bands in nanocrystalline iron with a grain size of 80 nm revealed a formation of crystallographic texture and strongly elongated grains [14]. This indicates the mechanism of SB formation similar to that in coarse-grained materials. It is very unlikely that this dislocation-based mechanism of shear band formation is active in the nanocrystalline Pd10Au alloy. First, the microstructure remained very homogenous with equiaxed grains (Fig. 1c). Second, the initial material was practically free of texture [25]. Further, shear bands appeared relatively early after the onset of full plasticity when strain was not sufficient to promote necessary lattice rotations by dislocation slip. This is confirmed by the present in situ synchrotron XRD measurements, which revealed very weak texture formation during compression (Fig. 6). Note that the XRD beam spot was large enough ( $8 \times 20 \mu\text{m}$ ), and for the typical spacing between shear bands it is unlikely that it could “miss” the sample volumes containing shear bands (note also that XRD investigation was performed in transmission mode, i.e., the whole sample thickness was analyzed). Hence, it is rather possible that shear banding results from grain boundary mediated deformation mechanisms. Indeed the spreading of shear bands over hundreds of microns (Fig. 4d, e) indicate that thousands of grains shift collectively. This implies that grain boundary sliding occurs in a cooperative manner [2, 28, 39]. Conversely, this does not exclude some additional

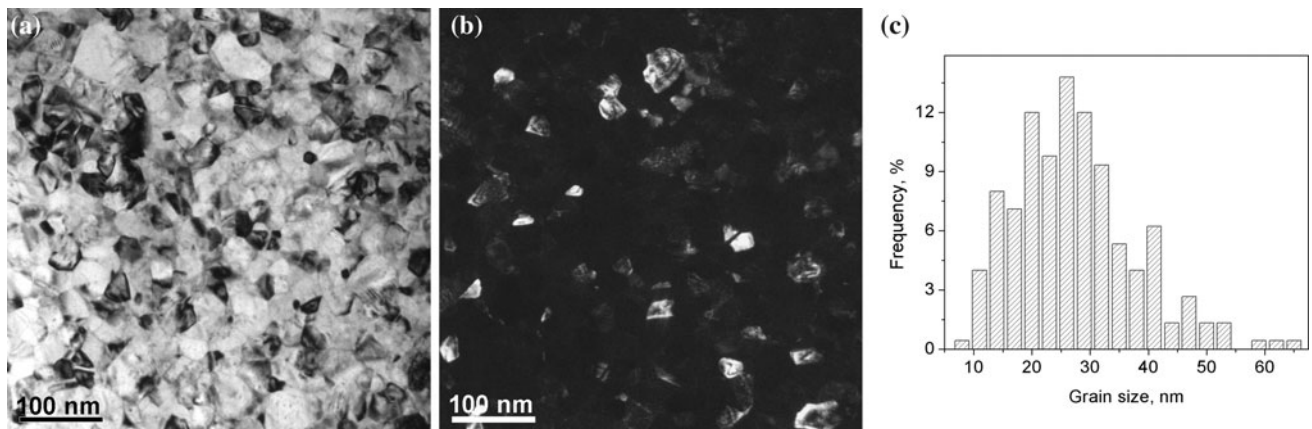


**Fig. 6** Microstructure of the nc Pd10Au alloy after compression test in area with maximal shear band density, **a** bright and **b** dark field TEM images, **c** grain size distribution

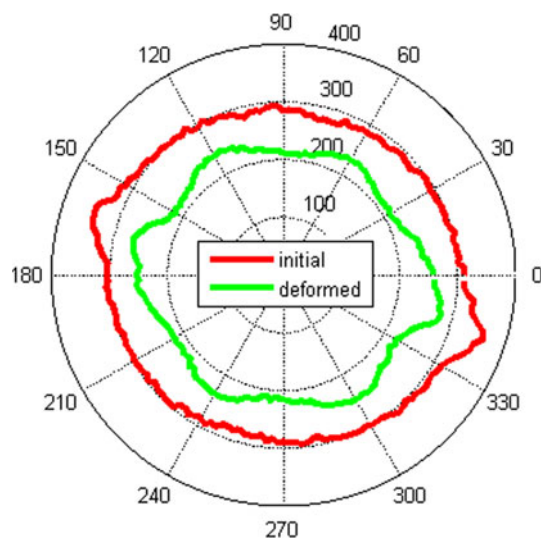


**Fig. 7** Polar plot of the modulation of the (111) integral peak intensity along the corresponding Debye–Scherrer ring of the nanocrystalline igc + hpt Pd10Au sample in the initial state and after 10 % compression

dislocation activity in the nc grains. The slight intensity redistribution indicates some degree of texture formation (Fig. 6), which is in agreement with our previous texture measurements in the same alloy after high-pressure torsion [25], as well as in experiments of other authors [5]. The texture evolution, however, is much weaker in comparison to other cases where dislocation glide is the governing deformation mechanism [40]. This is not surprising because grain boundary sliding requires accommodation, which at room temperature is rather realized by dislocation slip than via diffusive processes.

Generally, it looks like the deformation of nanocrystalline Pd10 Au alloy can be interpreted as an interplay of different deformation mechanisms: cooperative grain boundary sliding allows for dominant shear banding which

is accompanied by a minor contribution of dislocation plasticity and some stress driven grain boundary migration.

## Summary

Nanocrystalline Pd10Au alloy with a mean grain size of 23 nm was produced by inert gas condensation combined with subsequent high-pressure torsion. Monitoring the nc sample surface during in situ SEM compression testing revealed extended shear bands formation and strain softening.

We observed no modification of the microstructure of the alloy in areas with maximal shear band density (except slight increase of the mean grain size from 23 to 27 nm) and a negligible formation of crystallographic texture. Hence, we proposed that such behavior can be explained by the activation of grain boundary mediated deformation mechanisms instead of dislocation-based plasticity.

**Acknowledgements** This study was supported by Deutsche Forschungsgemeinschaft (FOR 714). The nanocrystalline igc Pd10Au base material was produced by the group of Prof. Rainer Birringer (FR7.2 Experimentalphysik, Universität des Saarlandes). The Karlsruhe Nano Micro Facility (KNMF) is gratefully acknowledged. We would like to thank Stephanie Kobler for help with editing this manuscript.

## References

1. Van Swygenhoven H, Derlet P (2001) *Phys Rev B* 64:224105
2. Hahn H, Mondal P, Padmanabhan KA (1997) *Nanostruct Mater* 9:603
3. Benkassem S, Capolungo L, Cherkaoui M (2007) *Acta Mater* 55:3563
4. Ma E (2004) *Science* 305:623
5. Shan Z, Stach EA, Wiezorek JMK, Knapp JA, Follstaedt DM, Mao SX (2004) *Science* 305:624

6. Chinh NQ, Szommer P, Horita Z, Langdon TG (2006) *Adv Mater* 18:34
7. Karch J, Birringer R, Gleiter H (1987) *Nature* 350:556
8. Liao XZ, Zhou F, Laverina EJ, Srinivasan SG, Baskes MI, He DW, Zhu YT (2003) *Appl Phys Lett* 83:632
9. Rosner H, Boucharat N, Markmann J, Padmanabhan KA (2010) *Acta Mater* 58:2610
10. Benkassem S, Capolungo L, Cherkaoui M (2007) *Acta Mater* 55:3563
11. Asaro RJ, Suresh S (2005) *Acta Mater* 53:3369
12. Wolf D, Yamakov V, Phillpot SR, Mukherjee A, Gleiter H (2005) *Acta Mater* 53:1
13. Carsley JE, Fisher A, Milligan WW, Aifantis E (1998) *Metall Trans A* 29:2261
14. Wei Q, Jia D, Ramesh KT, Ma E (2002) *Appl Phys Lett* 81:1240
15. Cheng S, Ma E, Wang YM, Kecskes LJ, Youssef KM, Koch CC, Trociewitz UP, Han K (2005) *Acta Mater* 53:1521
16. Koch CC (2003) *Scripta Mater* 49:657
17. Ma E (2006) *JOM* 58(4):49
18. Meyers MA, Mishra A, Benson DJ (2006) *Prog Mater Sci* 51:427
19. Kumar KS, Van Swygenhoven H, Suresh S (2003) *Acta Mater* 51:5743
20. Dao M, Lu L, Asaro RJ, De Hosson JTM, Ma E (2007) *Acta Mater* 55:4041
21. Hugo RC, Kung H, Weertman JR, Mitra R, Knapp JA, Follstaedt DM (2003) *Acta Mater* 51:1937
22. Kobler A, Kashiwar A, Hahn H, Kübel C (2013) *Ultramicroscopy* 128:68
23. Rösner H, Boucharat N, Markmann J, Padmanabhan KA, Wilde G (2009) *Mater Sci Eng A* 525:102
24. Budrovic Z, Van Swygenhoven H, Derlet PM, Van Petegem S, Schmitt B (2003) *Science* 304:273
25. Ivanisenko Yu, Skrotzki W, Chulist R, Lippmann T, Kurmanaeva L, Fecht H-J (2010) *J Mater Sci* 45:4571. doi:[10.1007/s10853-010-4552-y](https://doi.org/10.1007/s10853-010-4552-y)
26. Ivanisenko Yu, Skrotzki W, Chulist R, Lippmann T, Kurmanaeva L (2012) *Scripta Mater* 66:131–134
27. Birringer R, Gleiter H, Klein H-P, Marquardt P (1984) *Phys Lett A* 102:365
28. Ivanisenko Yu, Kurmanaeva L, Weissmueller J, Yang K, Markmann J, Rösner H, Scherer T, Fecht H-J (2009) *Acta Mater* 57:3391
29. Kurmanaeva L, Ivanisenko Yu, Markmann J, Yang K, Fecht H-J, Weissmüller J (2010) *Phys Status Solidi RRL* 4(5–6):130
30. Lohmiller J, Grewer M, Braun C, Kobler A, Kuebel C, Schueler K, Honkimäki V, Hahn H, Kraft O, Birringer R, Gruber PA (2013) *Acta Mater* (under review)
31. Ames M, Grewer M, Braun C, Birringer R (2012) *Mater Sci Eng A* 546:248
32. Saada G, Verdier M, Dirras GF (2007) *Philos Mag* 87:4875
33. Saada G, Kruml T (2011) *Acta Mater* 59:2565
34. Brandstetter S, Van Swygenhoven H, Derlet P, Van Petegem S, Schmitt B, Maaß R, Derlet PM (2006) *Adv Mater* 18:1545
35. Schwaiger R, Moser B, Dao M, Chollacoop N, Suresh S (2003) *Acta Mater* 51:5159
36. Legros M, Gianola DS, Hemker KJ (2008) *Acta Mater* 56:3380
37. Meyers MA (1994) *Dynamic Behavior of Materials*. Wiley, New York
38. Anand L, Kalidindi SR (1994) *Mech Mater* 17:223
39. Astanin VV, Sisanbaev AV, Pshenichnyuk AI, Kaibyshev O (1997) *Scripta Metall Mater* 36:117
40. Wassermann G, Grewen J (1962) *Texturen metallischer Werkstoffe*. Springer, Berlin